Coda-wave Interferometry Analysis of Time-lapse VSP Data for Monitoring Geological Carbon Sequestration

Authors: Rongmao Zhou [(1)], Lianjie Huang [(1)], James T. Rutledge [(1)]

Michael Fehler [(2)]

Thomas M. Daley [(3)] and Ernest L. Majer [(3)]

Affiliation:

(1) Geophysics Group, Los Alamos National Laboratory, Los Alamos, NM 87545

(2) Massachusetts Institute of Technology

(3) Lawrence Berkeley National Laboratory, Berkeley, CA 94720

Address:

(1) Geophysics Group, MS D443
Los Alamos National Laboratory
Los Alamos, NM 87545

(2) Department of Earth, Atmospheric, & Planetary Sciences
Massachusetts Institute of Technology
77 Massachusetts Avenue, 54-524
Cambridge, MA 02139

(3) Geophysics Department, MS 90-1116
Lawrence Berkeley National Laboratory
Berkeley, CA 94720

Email:

rongmaozhou@gmail.com (R. Zhou)
ljh@lanl.gov (L. Huang)
jrutledge@lanl.gov (J. Rutledge)
fehler@mit.edu (Michael Fehler)
tmdaley@lbl.gov (Thomas Daley)
elmajer@lbl.gov (Ernest Majer)

Fax: 1-505-667-8487

Coda-wave Interferometry Analysis of Time-lapse VSP Data for Monitoring Geological Carbon Sequestration

ABSTRACT

Injection and movement/saturation of carbon dioxide (CO_2) in a geological formation will cause changes in seismic velocities. We investigate the capability of coda-wave interferometry technique for estimating CO_2-induced seismic velocity changes using time-lapse synthetic vertical seismic profiling (VSP) data and the field VSP datasets acquired for monitoring of injected CO_2 in a brine aquifer in Frio, Texas, USA. Synthetic VSP data are calculated using a finite-difference elastic-wave equation scheme and a layered model based on the elastic Marmousi model. A possible leakage scenario is simulated by introducing seismic velocity changes in a layer above the CO_2 injection layer. We find that the leakage can be detected by the detection of a difference in seismograms recorded after the injection compared to those recorded before the injection at an earlier time in the seismogram than would be expected if there was no leakage. The estimated mean velocity changes, from both synthetic and field VSP data, increase significantly for receiver positions approaching the top of a CO_2 reservoir. Our results from field data suggest that the velocity changes caused by CO_2 injection could be more than 10% and are consistent with results from a crosswell tomogram study. This study demonstrates that time-lapse VSP with coda-wave interferometry analysis can reliably and effectively monitor geological carbon sequestration.

KEY WORDS

Coda-Wave Interferometry, Geologic Carbon Sequestration, Time-lapse VSP Monitoring, Vertical Seismic Profiling

INTRODUCTION

The goal of geological carbon sequestration is to permanently store large quantities of carbon dioxide (CO_2) within underground rock formations. It will be required to know with a high level of confidence that the injected CO_2 remains sequestered permanently. Seismic monitoring could play an important role to monitor and ensure safe, effective storage of CO_2. Time-lapse seismic reservoir monitoring is a process to acquire and analyze multiple seismic surveys, repeated at the same site over time, in order to image fluid-flow effects in a producing reservoir. As fluid saturations and pressures in the reservoir change, the seismic reflection properties change accordingly (Lumley, 2001). Time-lapse seismic monitoring provides information about changes in temperature, pressure, and volume change in fluid property within reservoir pore spaces at two different calendar dates. Time-lapse imaging has been successfully applied by the oil industry for reservoir monitoring (Santos and Harris, 2007). The ability to monitor reservoir changes as a function of time by the use of seismic methods can lead to better location of production and infill wells and the possibility of locating unswept zones (Ross *et al.*, 1996).

A similar theoretical background can be applied to monitor geologic CO_2 sequestration and to detect possible leakage. Depleted oil reservoirs, saline aquifers, and un-mineable coal seams have been suggested as potential storage sites. CO_2 could permanently be stored within the rock pore spaces where oil/natural gas/water have been held for millions of years. Injection and movement/saturation of CO_2 in a geological formation will cause changes in seismic velocities

and attenuation, which result in changes in seismic-wave scattering and propagation. The changes in seismic velocities are believed to be associated jointly with changes in fluid saturation (CO_2 replacing water and oil) and in pressure (increase in pore pressure due to the injection process) (Harris *et al.*, 1996). Wang *et al.* (1998) investigated the effect of CO_2 floods on the seismic velocities in a carbonate rock (dolostone). They found that compressional-wave (P-wave) velocity V_P decreases from a minimum 3.0% to as high as 10.9%, while shear-wave (S-wave) velocity Vs decreases from 3.3% to 9.5% as the reservoir rocks are flooded with CO_2 under in-situ conditions. Their results show that the combined effects of pore pressure buildup and fluid substitution caused by CO_2 flooding make it feasible to monitor the CO_2 flood process and to map the flooded zones seismically. Rock and fluid physics measurements and modeling suggest that CO_2 can cause a 4-6% decrease in V_P with a corresponding 15-20% change in reflection amplitude. Time-lapse surface seismic and vertical seismic profiling (VSP) surveys for monitoring CO_2 sequestration also showed changes in P-wave and S-wave velocities due to CO_2 injection and strong reflections from injection regions (Arts *et al.*, 2004; Daley *et al.*, 2007). Time-lapse crosswell tomograms show P-wave reductions of more than 10% in some formations within the reservoir zone and some changes are as large as 20% (Harris *et al.*, 1996, Daley et al, 2007).

The usefulness of temporal changes, however, is limited by the accuracy and precision with which velocity measurements can be made (Poupinet et al., 1984; Roberts *et al.*, 1992, Sneider et al., 2002). Poupinet et al., (1984) introduced the coda-wave interferometry method for estimating nonlinear behavior in seismic velocity. It has been applied to different studies, such as probing the relative location of seismic sources (Snieder and Vrijlandt, 2005), monitoring of rapid

temporal change in a volcano (Grêt *et al.*, 2005), and time-lapse monitoring of rock properties in a laboratory environment (Grêt *et al.*, 2006). The coda-wave interferometry method can be used to detect spatially localized changes using single scattering (Pacheco and Snieder, 2006) and multiple scattering (Pacheco and Snieder, 2005).

The purpose of this study is to explore the capability of the coda-wave interferometry method for monitoring geologic carbon sequestration. We use it to estimate seismic velocity changes due to CO_2 injection using synthetic and field time-lapse VSP data. The coda waves in upgoing VSP data are waves that have been multiply scattered from geologic layers below the receiver positions. First, we will briefly outline the coda-wave interferometry methodology, and using repeating earthquake events to validate the algorithm and explore the effects of temporal windows on the results of estimation. Then, we will apply the coda-wave interferometry methodology to synthetic time-lapse VSP data for monitoring CO_2 injection, and investigate the monitoring of the possible CO_2 leakage scenario. We will also apply the coda-wave interferometry method to the field time-lapse VSP datasets acquired for monitoring CO_2 injection into a brine aquifer in Frio, Texas, USA.

METHODOLOGY AND VALIDATION OF THE ALGORITHM

Poupinet et al., (1984) first proposed to measure small changes in coda waves to infer small changes in velocity of a region. Later, Snieder *et al.* (2002) proposed a method termed “Coda Wave Interferometry” for detecting the presence of temporal changes in the medium. Here we

briefly outline the coda-wave interferometry technique; more detailed information can be found in Snieder *et al.* (2002). Suppose that a strongly scattering medium is excited by a repeatable source, and that the medium changes with time. Before the change in the medium occurs, the unperturbed wave field $u^{(u)}(t)$ can be written as

$$u^{(u)}(t) = \sum_T A_T(t) , \tag{1}$$

which is a sum of waves propagating along the multiple scattering trajectories T in the medium, where t denotes time and $A_T(t)$ is the wave propagating along trajectory T. When the medium velocity changes over time, the dominant effect is a change τ_T in the arrival times of the waves that propagate along different trajectory T, so that the perturbed wave field is given by

$$u^{(p)}(t) = \sum_T A_T(t - \tau_T) . \tag{2}$$

The change in the waveforms can be quantified by computing the time-shifted cross-correlation over a time window at center time t with temporal width $2t_w$:

$$R(t_S) \equiv \frac{\int_{t-t_w}^{t+t_w} u^{(u)}(t') u^{(p)}(t' + t_S) dt'}{(\int_{t-t_w}^{t+t_w} (u^{(u)}(t'))^2 dt' \int_{t-t_w}^{t+t_w} (u^{(p)}(t'))^2 dt')^{1/2}} , \tag{3}$$

where t_S is the time shift of the perturbed waveform relative to the unperturbed one. When the waves are not perturbed, $u^{(p)}(t) = u^{(u)}(t)$, and the time-shifted cross-correlation is equal to unity for a zero lag time $R(t_S = 0) = 1$. When the perturbed wave within the measurement time window is a time-shifted version of the original wave, $u^{(p)}(t) = u^{(u)}(t - \tau)$, and $R(t_S)$ attain its maximum at $t_S = \tau$. In general, the time-shifted cross-correlation $R(t_S)$ attains its maximum at

a time $t_S = t_{\max}$ when

$$t_{\max} = \tau \, . \tag{4}$$

The shift time is given by the average perturbation of the travel time of the waves that arrive in the employed time window. For each time interval, the time shift between the perturbed and unperturbed waves is determined by computing the time-shifted cross-correlation in equation (3) and by picking the time for which the cross-correlation coefficient attains its maximum at $t_{\max}$. The relative velocity change for each time interval is the given by

$$\frac{\delta v}{v} = -\frac{t_{\max}}{t} = -\frac{\tau}{t}. \tag{5}$$

This velocity change is a function of the center time *t* of the employed time windows.

For spatially localized changes, the average or mean travel time change is given the by (Pacheco and Snieder, 2005):

$$\langle \tau(t) \rangle = -\int_V K(r',t) \frac{\delta v(r')}{v(r')} dV(r'), \tag{6}$$

where $\langle \tau(t) \rangle$ is the mean travel time change of the multiply scattering waves at travel time *t* due to the spatially localized velocity change $\frac{\delta v(r')}{v(r')}$ within the volume *V*, and $K(r',t)$ is the integration kernel satisfying

$$t = \int_V K(r',t) dV(r'). \tag{7}$$

We define the mean velocity change $\langle \frac{\delta v}{v} \rangle$ as

$$\langle \frac{\delta v}{v} \rangle \equiv \frac{\int_V K(r',t) \frac{\delta v(r')}{v(r')} dV(r')}{\int_V K(r',t) dV(r')} = -\frac{\langle \tau(t) \rangle}{t}. \quad (8)$$

We use the mean velocity change $\langle \frac{\delta v}{v} \rangle$ for qualitative detection of reservoir changes due to CO_2 injection.

We implement the coda-wave interferometry algorithm in Matlab environment. To test the codes and explore the effects of parameters, such as temporal window length, on the results of velocity change estimations, we apply the coda-wave interferometry method to repeating earthquake events. The testing results indicate that a shorter window length (about 1~3 wave periods) have some fluctuations and include outliers at some center times. When the window length is greater than 4 wave periods, the results of the coda-wave interferometry are almost the same. The results validate our computer codes of the coda-wave interferometry method and show that the technique could be used to estimate the relative changes using seismic data with longer window lengths.

APPLICATION TO SYNTHETIC TIME-LAPSE VSP DATA

We first study the feasibility of the coda-wave interferometry method for monitoring geologic carbon sequestration using synthetic time-lapse VSP data. We also investigate whether this

technique could be used to detect the possible leakage scenario from the CO_2 injection, which is one of main tasks of monitoring geologic CO_2 sequestration. We use layered elastic models (P-wave velocity: V_P; S-wave velocity: V_S; and density: ρ) to calculate synthetic VSP seismograms (Fig. 1). The reference layered model is based on a portion of the elastic Marmousi model (Martin *et al.*, 2006) without the top water layers (Fig. 1). The VSP source and receiver geometries for the synthetic seismogram calculations are depicted in Fig. 1. The red star denotes the source; red triangles are receivers; and the green filled rectangle represents the CO_2 injection layer with a thickness of 200 m. The VSP offset is 1000 m and the source is located 50 m below the surface. The synthetic VSP data calculated using the reference model are used as the pre-injection, baseline VSP data. To obtained post-injection synthetic VSP data, we change the velocities values in the CO_2 injection layer (the green layer in Fig. 1) and the resulting model is called Test Model 1. Rock and fluid physics measurements and modeling suggest that CO_2 can cause a 4-6% decrease in P-wave velocity and a 5-10% decrease in S-wave velocity (Davis *et al.*, 2003). Test Model 1 has 6% decrease in P-wave velocity and 5% decrease in S-wave velocity relative to the reference model. To simulate a possible leakage scenario, Test Model 2 is created by changing model parameters in a layer (cyan) above the CO_2 injecting layer (green). Test Model 2 for the leakage scenario contains an additional leakage layer with 3% P-wave velocity decrease and 3% S-wave velocity decrease relative to Test Model 1.

A finite-difference elastic-wave-equation scheme (Cheng, 1994; Kamm *et al.*, 1996) is used to calculate synthetic seismograms for an explosive point source with a center frequency of 25Hz. P and S waves were separated using divergence and curl of the wavefield (Sun and McMechan, 2001). Upgoing and downgoing wavefield separation is accomplished in the frequency-

wavenumber (*f*-*k*) domain using the technique of contour-slice filtering (Suprajitno and Greenhalgh, 1985; Hardage, 2000). Since most of the downgoing wavefield does not pass through the injection layer, we only use upgoing waves for our monitoring studies. Figure 2 shows the upgoing waves of synthetic seismograms for the reference model (upper-left) and the Test Model 1 (upper-right). The upgoing waves for the Test Model 1 at receiver #1, #201, #401, #601, #801 and #1001 superposed with the waveforms from the reference model are also presented in Figure 2. The velocity change estimated using the coda-wave interferometry technique for time-lapse VSP data is the velocity change over the entire travel path. We calculate the temporal velocity changes at the centers of a moving time window using the coda-wave interferometry method, and then obtain the mean velocity change by averaging the temporal velocity changes over entire analyzed time record. Figure 3 presents the comparison of results for Test Model 1 relative to the reference model (blue) and Test Model 2 (leakage scenario) relative to the reference model (red) at receivers #1, #201, #401, #601, #801 and #1001 as marked as solid blue triangles in Fig. 1. The estimated temporal velocity changes occur earlier for Test Model 2 compared to those for Test Model 1 at all receivers. The earlier occurrences of changes imply some velocity changes occurred in the upper layers over the injection layer, indicating CO_2 leakage.

For each receiver, we estimate the velocity change versus the time as the examples shown in Figure 3, then we average them over whole time window to obtain the mean velocity change for each receiver. Figure 4 shows the mean P-wave velocity change for each receiver versus the receiver depth with temporal window length of 5 periods for the central frequency; and Figure 5 presents estimated mean velocity changes of the S-wave. The mean velocity change increases

significantly when receivers approach the top of the CO_2 injection layers. The results for the leakage scenario show the overall contribution from the injection and leakage layers.

At each receiver position, the upgoing waves have propagated varying distances through the section, of which only a portion corresponds to the 200 m injection interval where the velocity change occurs. Therefore, the receivers with the maximum P-wave velocity changes are those near the injection layer since the 200 m interval makes up a larger fraction of the total travel paths over which change is being measured. The receivers with the maximum estimated P-wave velocity changes are those near the injection layer. For these receivers, the total lengths of wave propagation paths are around 2000 m, and the propagation paths within the injection layer are approximately 400 m, which are nearly 20% of the entire wavepaths. The maximum mean velocity changes for these receivers are approximate 0.6%, roughly 10% of the given changes in the models. After taking in account the effect of the propagation paths through the injection layer over the total paths, the estimated mean velocity changes are half of the input value. The maximum estimated changes from Test Model 2 are approximately 1.5 times bigger than results from Test Model 1, which is the same as given velocity changes ratios for both models relative to the reference model. These results reveal characteristics of the coda-wave interferometry as a detector of the relative temporal changes.

APPLICATION TO FIELD TIME-LAPSE VPS DATA

CO_2 Injection Test in Frio, Texas

The field time-lapse VSP data were collected in Frio for a small scale (1,600 ton) pilot test of CO_2 injection into a brine aquifer. The goals of the pilot study were to safely inject CO_2, model the expected CO_2 flow, sample the fluid in an up-dip observation well, and monitor the resulting CO_2 plume (Hovorka *et al*. 2006, Doughty *et al*. 2007). The selected aquifer is a part of the on-shore Gulf of Mexico Frio formation sandstone. The experimental site is in an oil field and an idle well was used as an observation well. A new well was drilled for injection about 30 m offset from the existing observation well.

Time-lapse VSP data were acquired using a tubing-deployed, 80-level, 3-component geophone string and explosive sources. The explosive shot holes were roughly 18.3 m (60 ft) deep and were located 130 m to 1500 m away from the instrumented injection well on multiple azimuths. Each shot contained 1.6 kg (3.5 lbs) of dynamite. The data analyzed here are from the source offset 130 m updip (north) from the injection well, This is the azimuth for which the propagation is most likely 2D (in the plane of source and sensors). The time-lapse VSP data were acquired in July 2004 (pre-injection survey) and in late November 2004 (post-injection surveys), which was 1.5 months after the CO_2 was injected into the upper C-sand of the Frio Formation at depth from 1,528.5 m to 1,534.7 m (Daley *et al.*, 2007).

Daley *et al.* (2007) described the steps of data processing for these dataset. After applying some standard VSP processing steps, that included frequency-wavenumber separation of downgoing and upgoing wavefield, and converting reflections to two-way travel time, the amplitudes were equalized using reflections from an interface above the reservoir as a reference. This equalization assumes that amplitude changes in reflectors above the injection interval are due to shallow sub-surface changes (such as soil moisture saturation) or changes in the seismic source amplitude.

Therefore, the amplitude change measured in the shallow reflector is subtracted from all the data. Figure 6 presents the pre- and post-injection up-going VSP data after these pre-process procedures from offset 1, which illustrates the high data quality.

Coda-wave interferometry analysis

The coda-wave interferometry method is applied to these pre- and post-injection VSP data to estimate seismic velocity changes caused by the CO_2 injection. The central frequency for these data is approximately 30 Hz. For the coda-wave interferometry analyses, we use a temporal window length of 0.198 and 0.297 sec, which is equivalent to 6 and 9 periods at the center frequency, respectively. The results are similar for both cases. Figure 7 presents the mean velocity changes versus the depth of VSP receivers with a time window length of 6 periods. The mean velocity change is nearly constant at geophones above 1400 m; increases significantly at receiver positions near the top of the CO_2 injection layer; and then decreases with increasing receiver depth below the injection layer.

Figure 7 shows that the maximum estimated velocity change is about 0.045%. The thickness of the injection layer was about 6.2 m (Daley *et al.*, 2007). By taking into account the relative ray path through the injection layer to the entire path of the upgoing waves, the actual average velocity change could be between 10% and 20%.

To verify the estimated velocity changes from the time-lapse VSP data, a genetic algorithm and ray tracing method are used to invert the velocity model from the picked first break times. The left panel of Fig. 8 shows a comparison of the picked travel times (red) and the calculated travel

times from one of the best inverted models on the right. We also compare the inverted velocity structure with the log data. The velocities below 1100 m fit well with the log data and the first-break time fit well for VSP receiver at all depth ranges. This inverted Vp model is used to calculate pre-injection VSP synthetic seismograms. Vs model is obtained from Vp according to the Vp/Vs ratio obtained from log data. The results from the cross-well tomogram study show seismic P-wave velocity decrease up to 500 m/s (Daley *et al.*, 2007) in the injection region. We change velocities in the injection layer by decreasing Vp by 200 m/s and Vs by 50 m/s, and use this modified model to calculate the post-injection VSP synthetic data. The synthetic VSP data are calculated using a finite-difference elastic-wave-equation scheme (Cheng, 1994; Kamm *et al.*, 1996) with an explosive source that has a center frequency of 30 Hz and is located 130 m away from the monitoring well (a similar geometry as the Frio field experiment).

Figure 9 is the comparison of estimated velocity changes from synthetic time-lapse (red) and field VSP (blue). Both estimated velocity changes reach a maximum near the injection layer with a value of approximately 0.045%. The results from time-lapse filed VSP data are consistent with those from synthetic VSP data with the mean P-wave velocity changes 200 m/sec in the injection layer.

CONCLUSIONS

We have investigated the feasibility of the coda-wave interferometry analysis for monitoring CO_2 injection and detecting a CO_2 leakage scenario using time-lapse VSP data. The coda-wave interferometry method can accurately determine the time in the seismograms when the temporal velocity change occurs for a given leakage scenario. If the center time of the first temporal velocity change shifts to earlier

portions of time-lapse seismograms, it indicates that some CO_2 could have leaked to the upper layers. This provides a quick and reliable tool for detecting CO_2 leakage using time-lapse VSP data. Synthetic study results suggest that the estimated relative temporal change is equivalent to the given changes after we take into account the ratio of the length of the wave path through the injection layer where velocity changes occur over the length of the entire propagation path. We have applied coda-wave interferometry to time-lapse field VSP data from the Frio project. The results from the field data indicate that the mean velocity changes caused by injecting CO_2 into the Frio Formation could be larger than 10%. This result is consistent with results from the time-lapse crosswell tomography study for the same field experiment. Our studies with synthetic and field time-lapse VSP data suggest that coda-wave interferometry analysis could be a reliable and effective tool for monitoring geological carbon sequestration.

ACKNOWLEDGEMENTS

This work was supported by the U.S. Department of Energy through contract DE-AC52-06NA25396 to Los Alamos National Laboratory. Field VSP data were collected by Lawrence Berkeley National Laboratory for the GEOSEQ project for the Assistant Secretary for Fossil Energy, Office of Coal and Power Systems through the National Energy Technology Laboratory, of the U.S. Department of Energy, under contract No. DE-AC02-05CH11231.

REFERENCES

Arts, R., O. Eiken, A. Chadwick, P. Zweigel, L. van der Meer, B. Zinszner, 2004. Monitoring of CO_2 injected at Sleipner using time-lapse seismic data. *Energy* **29,** 1383-1392.

Cheng, N., 1994. Borehole wave propagation in isotropic and anisotropic media: three-dimension finite difference approach, *Ph.D. Thesis*, Massachusetts Institute of

Technology.

Davis, T. L., M. J. Terrell, R. D. Benson, R. Cardona, R. R. Kendall, R. Winarsky, 2003. Multicomponent seismic characterization and monitoring of CO_2 flood at Weyburn Field, Saskatchewan. *The Leading Edge* **22,** 696-697.

Daley, T.M, L.R. Myer, E.L. Majer, J.E. Peterson, 2005. Acquisition of time-lapse, 6-component, P- and S-wave, crosswell seismic survey with orbital vibrator, and of time-lapse VSP for CO2 injection monitoring, 75th Ann. Internat. Mtg., Soc. Expl. Geophys., Expanded Abstracts, 1277-1279.

Daley, T. M., L. R. Myer, J. E. Peterson, E. L. Majer and G. M. Hoversten, 2007. Time-lapse crosswell seismic and VSP monitoring of injected CO_2 in a brine aquifer, *Environ. Geol.* DOI 10.1007/s00254-007-0943-z.

Doughty, C., B. M. Freifeld, R. C. Trautz, 2007. Site characterization for CO_2 geologic storage and vice versa: the Frio brine pilot, Texas, USA as a case study, *Environ. Geol.* DOI 101007/s00254-007-0942-0.

Grêt, A., R. Snieder, R. C. Aster, P. R. Kyle, 2005. Monitoring rapid temporal change in a volcano with coda wave interferometry, *Geophys. Res. Lett.* **32,** L06304, doi:10.1029/2004GL021143.

Grêt, A., R. Snieder, J. Scales, 2006. Time-lapse monitoring of rock properties with coda wave interferometry, *J. Geophys. Res.* 111, B03305, doi: 10.1029/2004JB003354.

Harris, J. M., R., T. Langan, T. Fasnacht, D. Melton, B. Smith, J. Sinton, H. Tan, 1996. Experimental verification of seismic monitoring of CO2 injection in carbonate reservoirs, 66th Ann. Internat Mtg., Soc. Expl. Geophys., Expended Abstracts, 1870-1872.

Hardage, B. A., 2000. *Handbook of Geophysical Explosion*, Vol. 14: Vertical Seismic Profiling:

Principles, third updated and revised edition, Elsevier Science Ltd.

Hovorka, S D., S. M. Benson, C. Doughty, B. M. Freifeld, S. Sakuriai, T. M. Daley, Y. K.Kharaka, M. H. Holtz, R. C. Trautz, H. S. Nance, L. R. Myer, K.G. Knauss, 2006. Measuring permanence of CO_2 storage in saline formations: the Frio experiment, *Environ. Geosci.* **13,** No. 2, 105-121.

Kamm, J. R., R. J. Bos, E. M. Jones, 1996. User's Guide to AFD v. 1.0, Los Alamos National Laboratory, LA-UR-96-853.

Lumley, D. E., 2001. Time-lapse seismic reservoir monitoring, *Geophysics* **66,** 50-53.

Martin, G. S., R. Wiley, K. J. Marfurt, 2006. Marmousi2: An elastic upgrade for Marmousi, *The Leading Edge.* **25,** 156-166.

Pacheco, C. and R. Snieder, 2005. Time-lapse time time change of multiply scattered acoustic waves, *J. Acoust. Soc. Am.* **118**, 1300-1310.

Pacheco, C. and R. Sneider, 2006. Time-lapse traveltime change of singly scattered acoustic waves, *Geophy. J. Int.* **165**, 485-500.

Poupinet, G., W. L. Ellsworth, and J. Frechet, 1984. Monitoring velocity variations in the crust using earthquake doublets: an application to the Calaveras Fault, California, *J. Geophy. Res.* **89,** 5719-5731.

Roberts, P. M., W. S. Phillips, M. C. Fehler, 1992. Development of the active doublet method for measuring small velocity and attenuation changes in solids, *J. Acoust. Soc. Am.* **91**, 3291-3302.

Ross, C. P., G. B. Cunningham, D. P. Weber, 1996. Inside the crossequalization black box, *The Leading edge* 15, 1233-1240.

Santos, E. T. F., J. M. Harris, 2007. Time-lapse diffraction tomography for trigonal meshes with temporal data integration applied to CO_2 sequestration monitoring, 77th Ann. Internat Mtg., Soc. Expl. Geophys, Expanded Abstracts, 2959-2963.

Snieder, R., A. Grêt, H. Douma, J. Scales, 2002. Coda wave interferometry for estimating nonlinear behavior in seismic velocity, *Science* **295,** 2253-2255.

Snieder, R., M. Vrijlandt, 2005. Constraining the source separation with coda wave interferometry: Theory and application to earthquake doublets in the Hayward fault, California, *J. Geophys. Res.*, 110, B04301, doi:10.1029/2004JB003317.

Sun, R. and G. A. McMechan, 2001. Scalar reverse-time depth migration of prestack elastic seismic data, *Geophysics* **66,** 1519-1527.

Suprajitno, M., S. A. Greenhalgh, 1985. Separation of upgoing and downgoing waves in vertical seismic profiling by contour-slice filtering, *Geophysics* **50,** 950-962.

Waldhauser, F., W. L. Ellsworth, 2002. Fault structure and mechanics of the Hayward Fault, California, from double-difference earthquake locations, *J. Geophys. Res.* **107,** B3, 2054, 10.1029/2000JB000084.

Wang, Z., M. E. Cates, R. L. Langan, 1998. Seismic monitoring of CO_2 flood in a carbonate reservoir: A rock physics study, *Geophysics* **63,** 1604-1617.

Figures Captions:

Figure 1. Left: The elastic Marmousi model (P-wave velocity:Vp; S-wave velocity: Vs and Density: ρ); Middle: A profile of the elastic Marmousi model at horizontal location 12000m (thin dotted lines on left) and a modified layered model (thick solid lines) used for synthetic seismogram calculations; Right: VSP geometry for synthetic seismogram calculations and a sketch of possible leakage scenario with parameters changes in the leakage layer (cyan) and the injection layer (green).

Figure 2. Synthetic seismograms of upgoing waves for the reference model (upper-left) and test model 1 (upper-right) at receiver #50, #100, #150, #200, …, #1000. Lower panel is the plot of the synthetic seismograms for the reference model (blue) superposing with synthetic seismograms for test model 1 (red) at receiver #1, #201, #401, #601, #801, #1001.

Figure 3. Temporal velocity changes estimated using the coda-wave interferometry technique from synthetic seismograms for test model 1 (solid blue line with crosses) and test model 2 (solid red with plus) relative to the reference model at receivers #1, #201, #401, #601, #801, #1001 (see Fig.1). The maximum correlation functions between the reference model and test model 1 (dotted blue with crosses), the reference model and test model 2 (dotted red with plus) at each moving window is ploted in each sub panel.

Figure 4. The estimated mean P-wave velocity change versus the receiver depth. The blue curve is for test model 1, and the red one is for test model 2 relative to the reference model. The

green layer is the CO_2 injection layer, and the cyan layer is a leakage layer.

Figure 5. The estimated mean S-wave velocity change versus the receiver depth. The blue curve is for test model 1, and the red one is for test model 2 relative to the reference model. The green layer is the CO_2 injection layer, and the cyan layer is a leakage layer.

Figure 6. Vertical component VSP seismograms recorded from shot 1 (Left: Pre-Injection; and Right: Post-Injection). The injection layer is marked as thick green line at depth range of 1528.5 and 1534.7 m.

Figure 7. The mean velocity change versus the receiver depth for the field time-lapse VSP data set. The thick green line indicates the CO_2 injection layer.

Figure 8. Left: Comparison of picked (red) first break time and calculated (blue) first break time from the inverted model on the right; Right: One of best fitting models inverted using genetic algorithms. Thick green line denotes the injection layer; cyan and magenta curves are the p-wave, and s-wave velocity log data, respectively.

Figure 9. Comparison of estimated velocity changes vs. VSP receiver depth for field VSP data (blue) and synthetic time-lapse VSP data (red) with P-wave velocity reduction 200 m/sec and S-wave velocity reduction 50 m/sec.

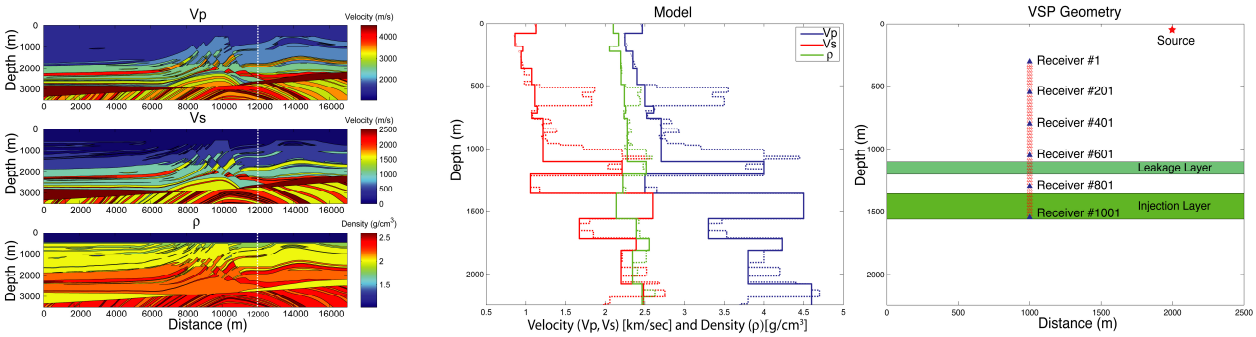

Figure 1.

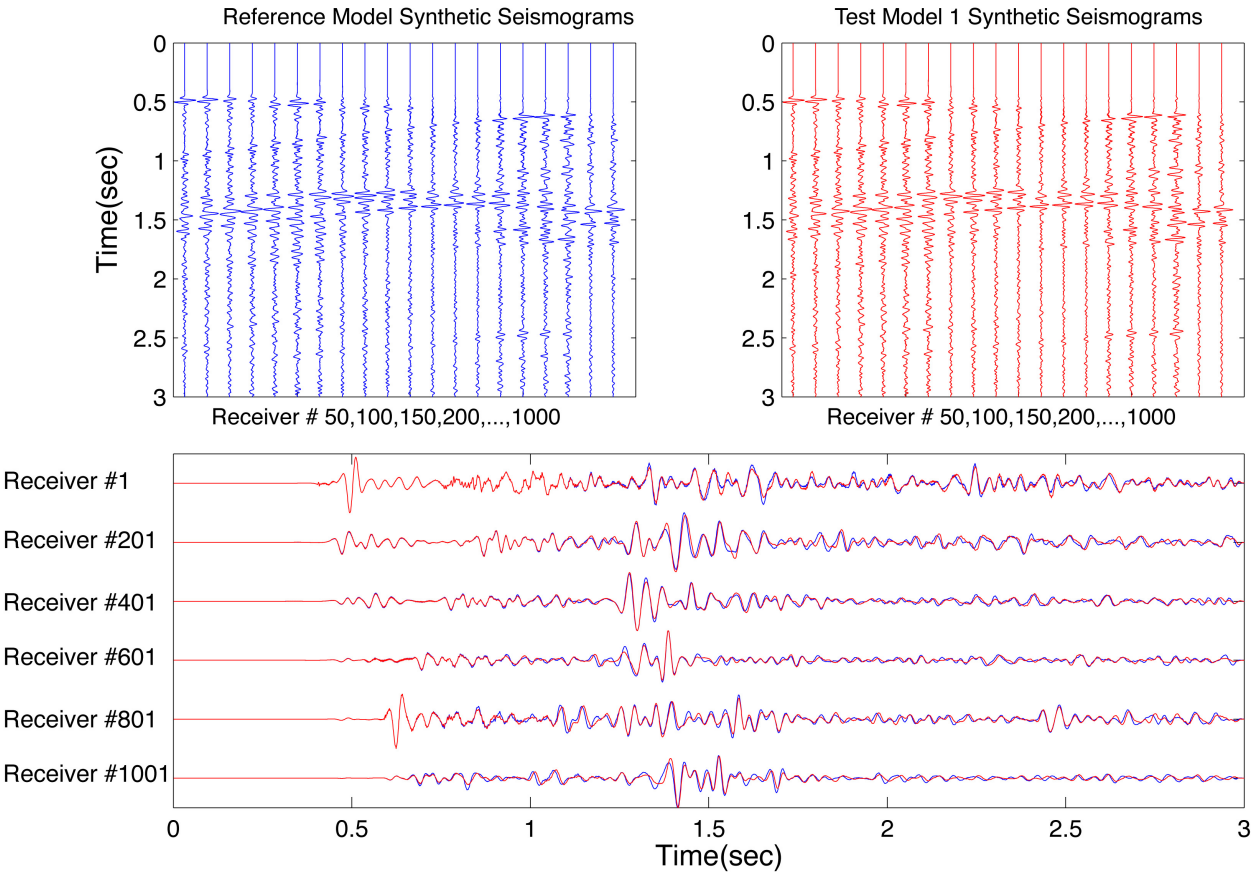

Figure 2.

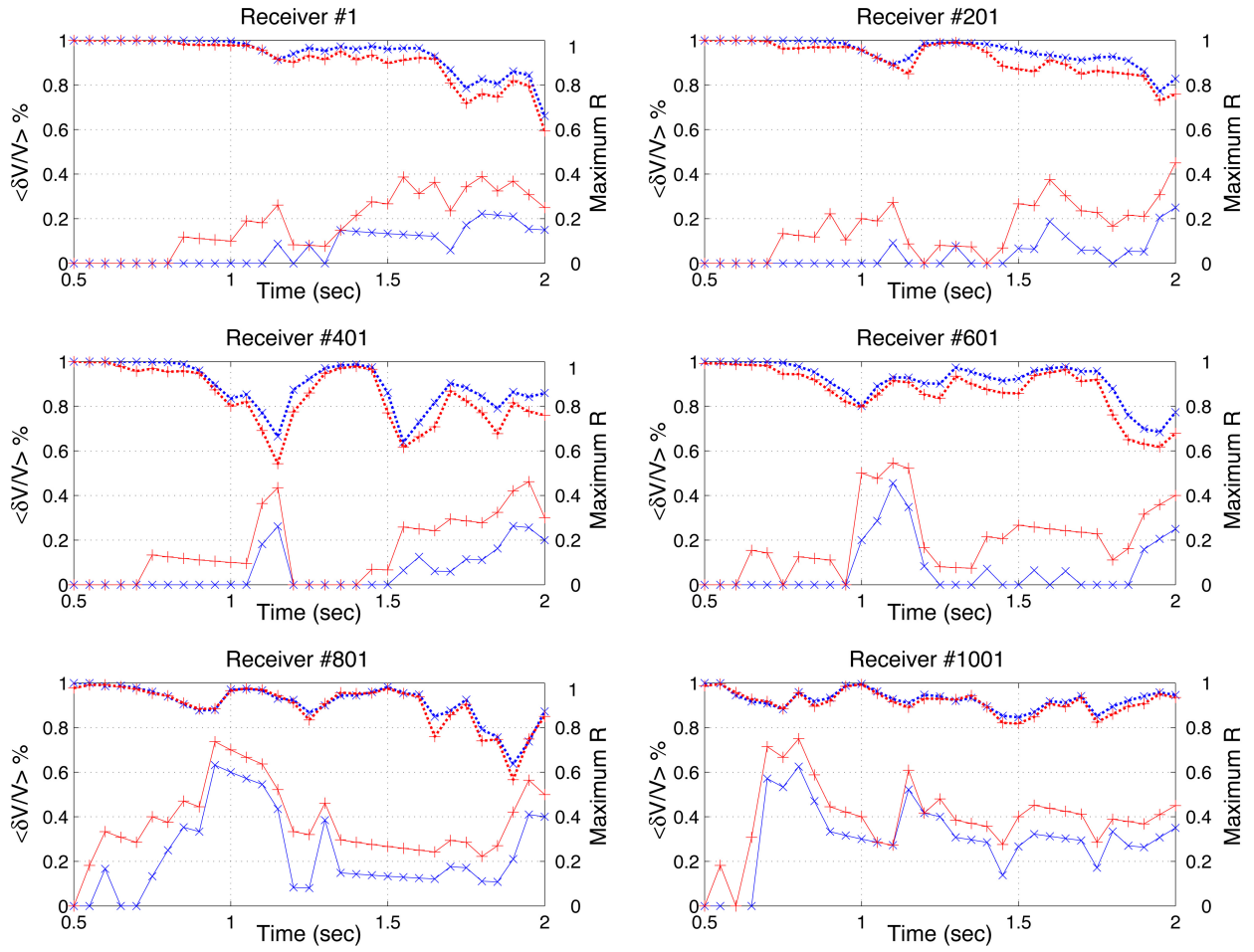
Receiver #1
Receiver #201
Receiver #401
Receiver #601
Receiver #801
Receiver #1001
<δV/V> %
Maximum R
Time (sec)

Figure 3.

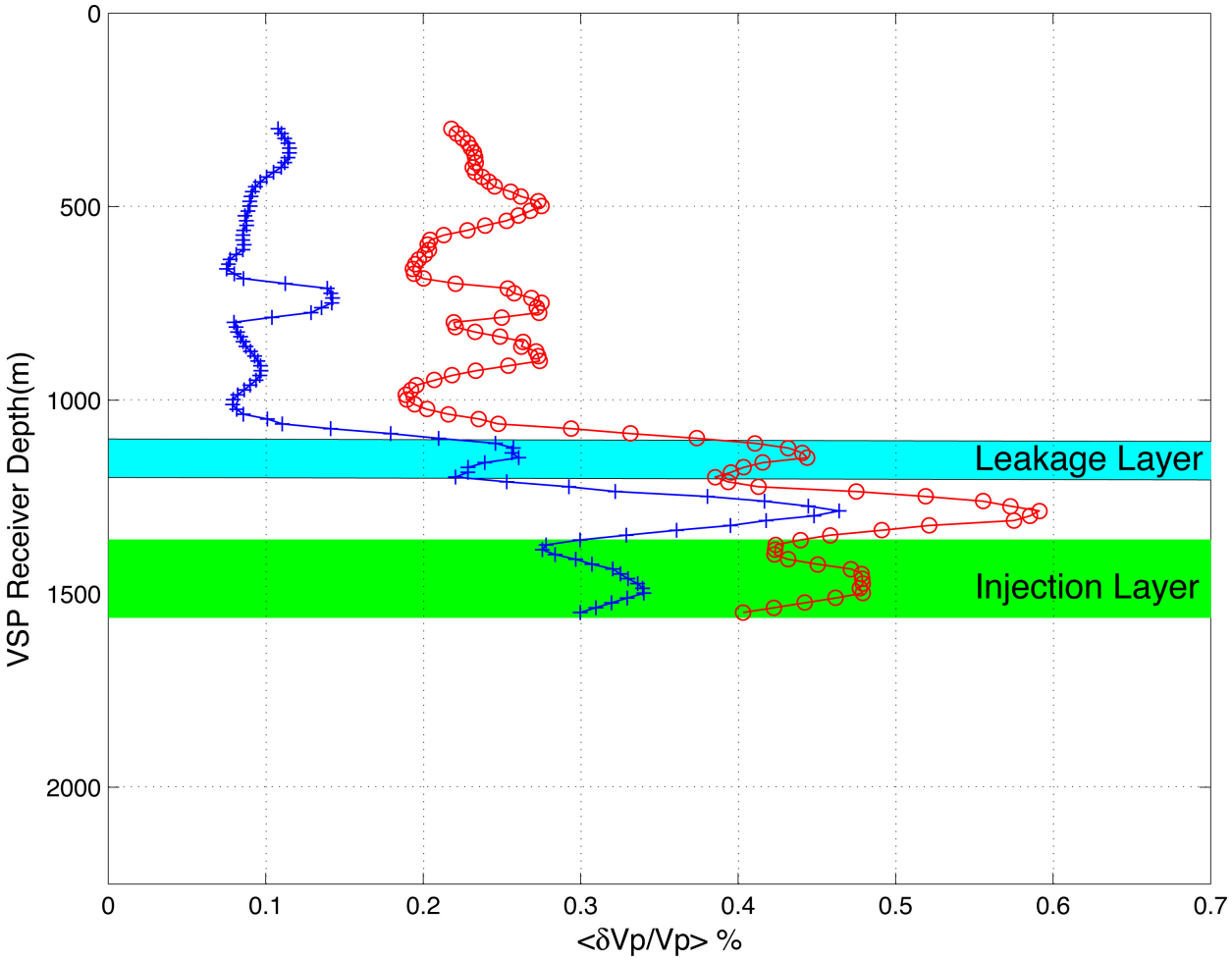
0
500
1000
1500
2000
VSP Receiver Depth(m)
0
0.1
0.2
0.3
0.4
0.5
0.6
0.7
<δVp/Vp> %
Leakage Layer
Injection Layer

Figure 4.

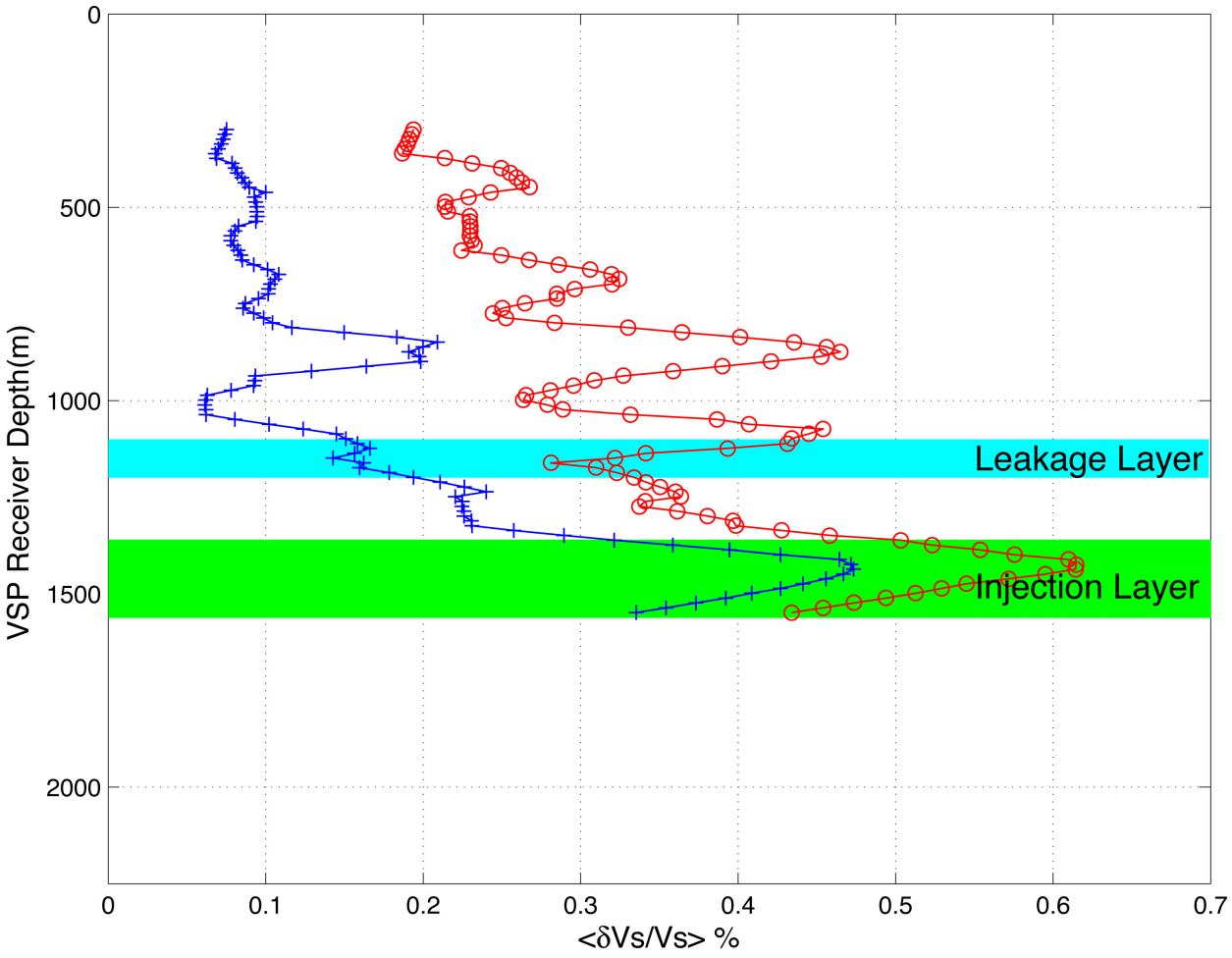
0
500
1000
1500
2000
VSP Receiver Depth(m)
0
0.1
0.2
0.3
0.4
0.5
0.6
0.7
<δVs/Vs> %
Leakage Layer
Injection Layer

Figure 5.

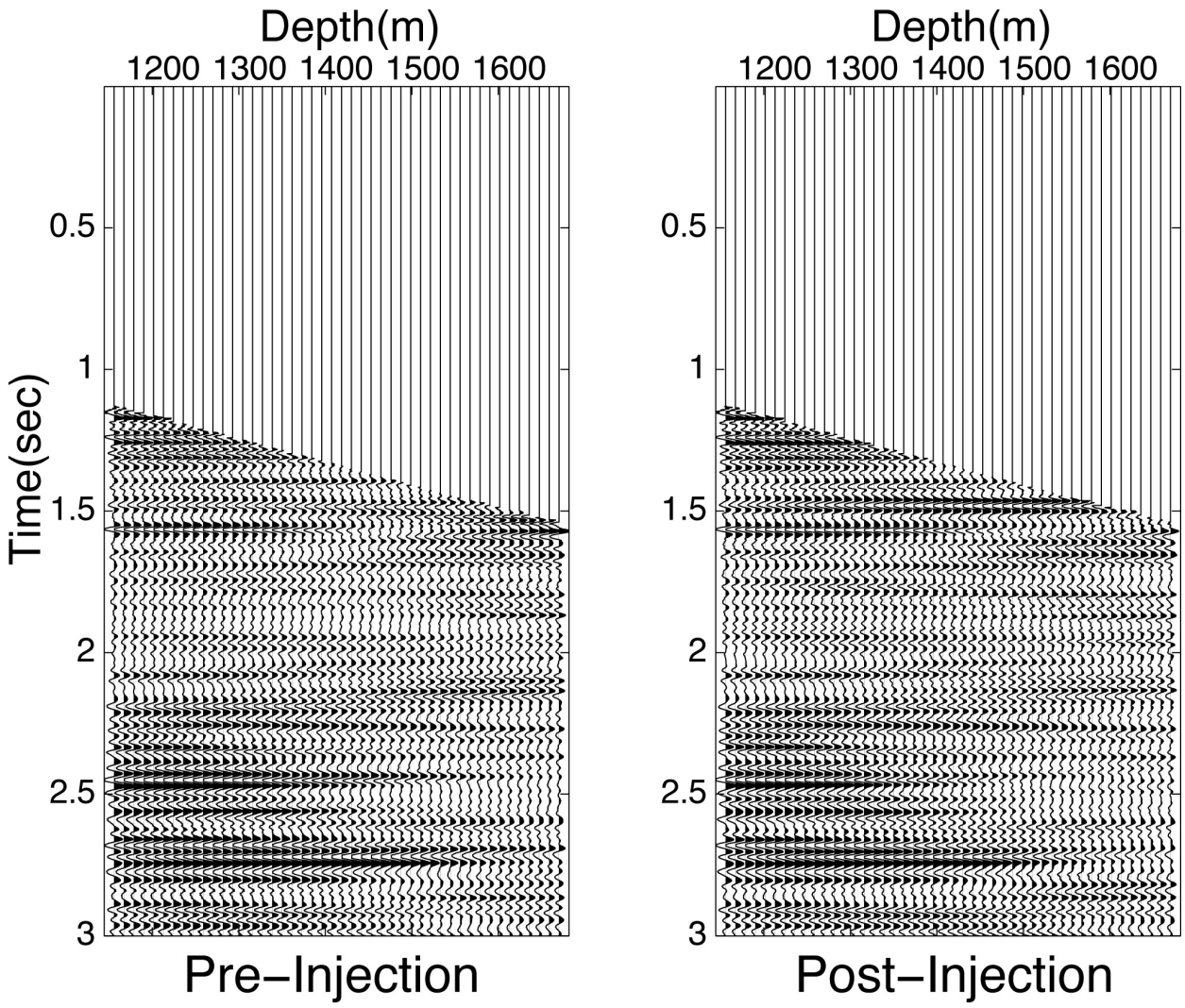
Depth(m)
1200 1300 1400 1500 1600
Time(sec)
0.5
1
1.5
2
2.5
3
Pre−Injection
Depth(m)
1200 1300 1400 1500 1600
0.5
1
1.5
2
2.5
3
Post−Injection

Figure 6.

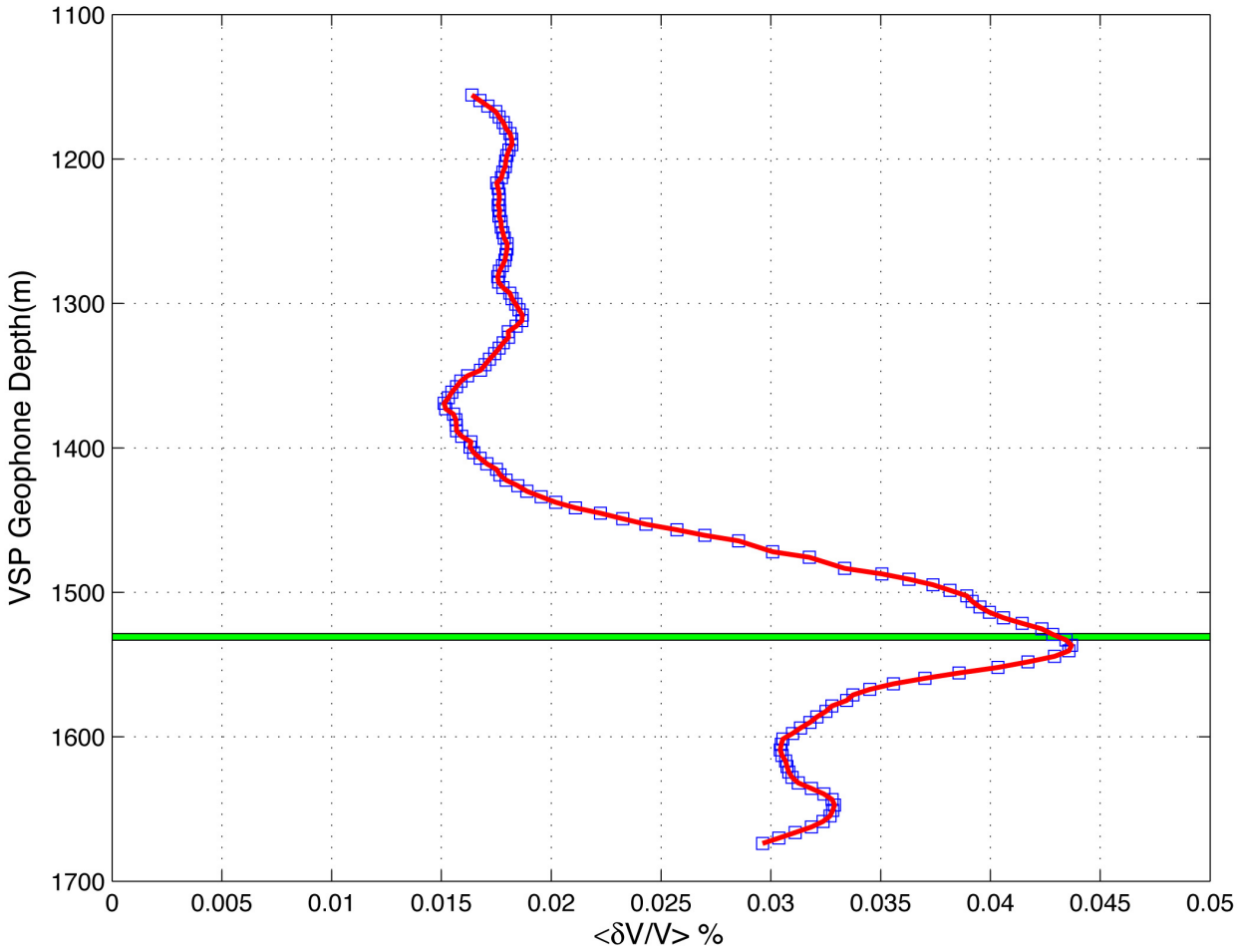
1100
1200
1300
1400
1500
1600
1700
VSP Geophone Depth(m)
0
0.005
0.01
0.015
0.02
0.025
0.03
0.035
0.04
0.045
0.05
<δV/V> %

Figure 7.

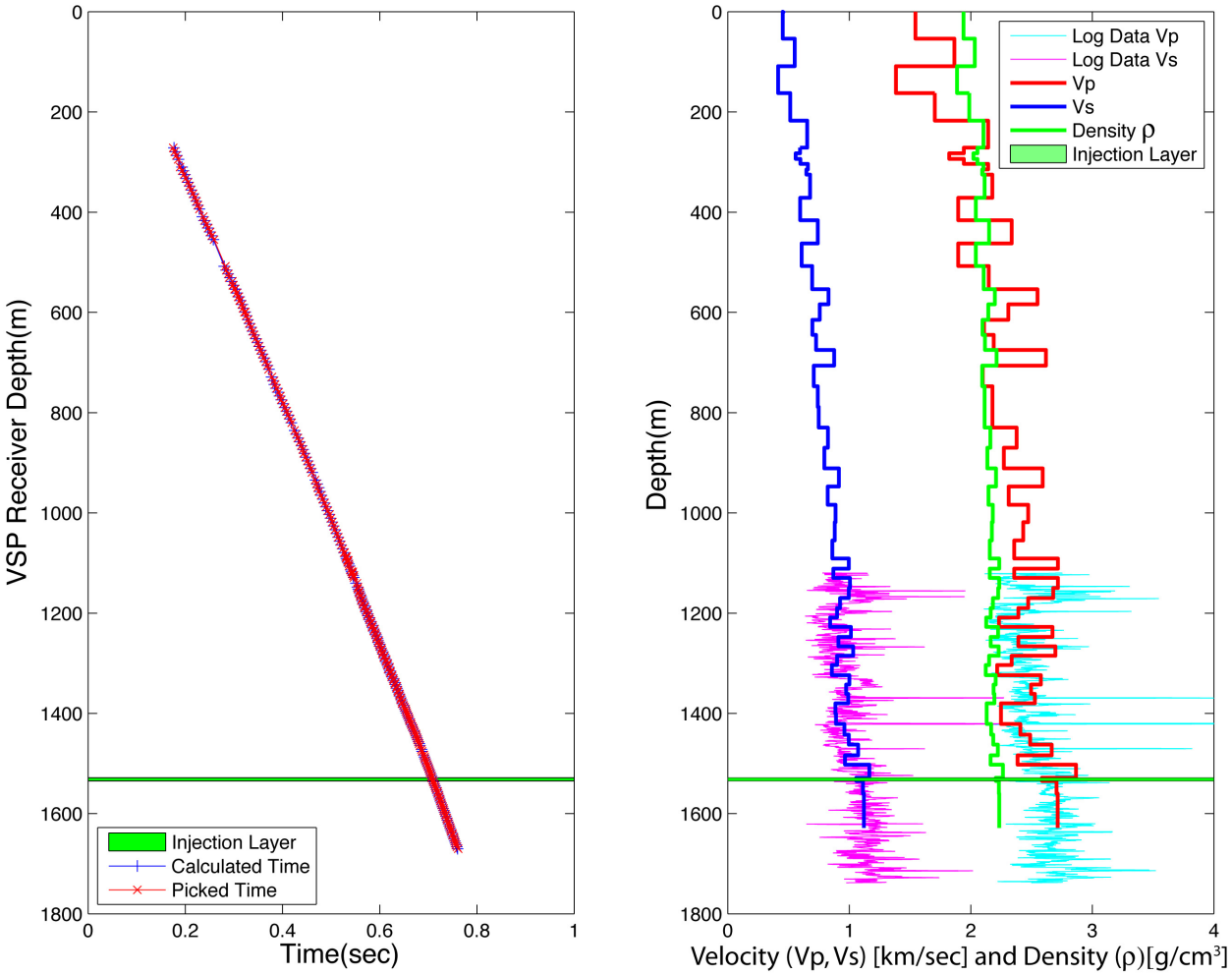
VSP Receiver Depth(m)
Time(sec)
Injection Layer
Calculated Time
Picked Time
Depth(m)
Velocity (Vp, Vs) [km/sec] and Density (ρ)[g/cm³]
Log Data Vp
Log Data Vs
Vp
Vs
Density ρ
Injection Layer

Figure 8.

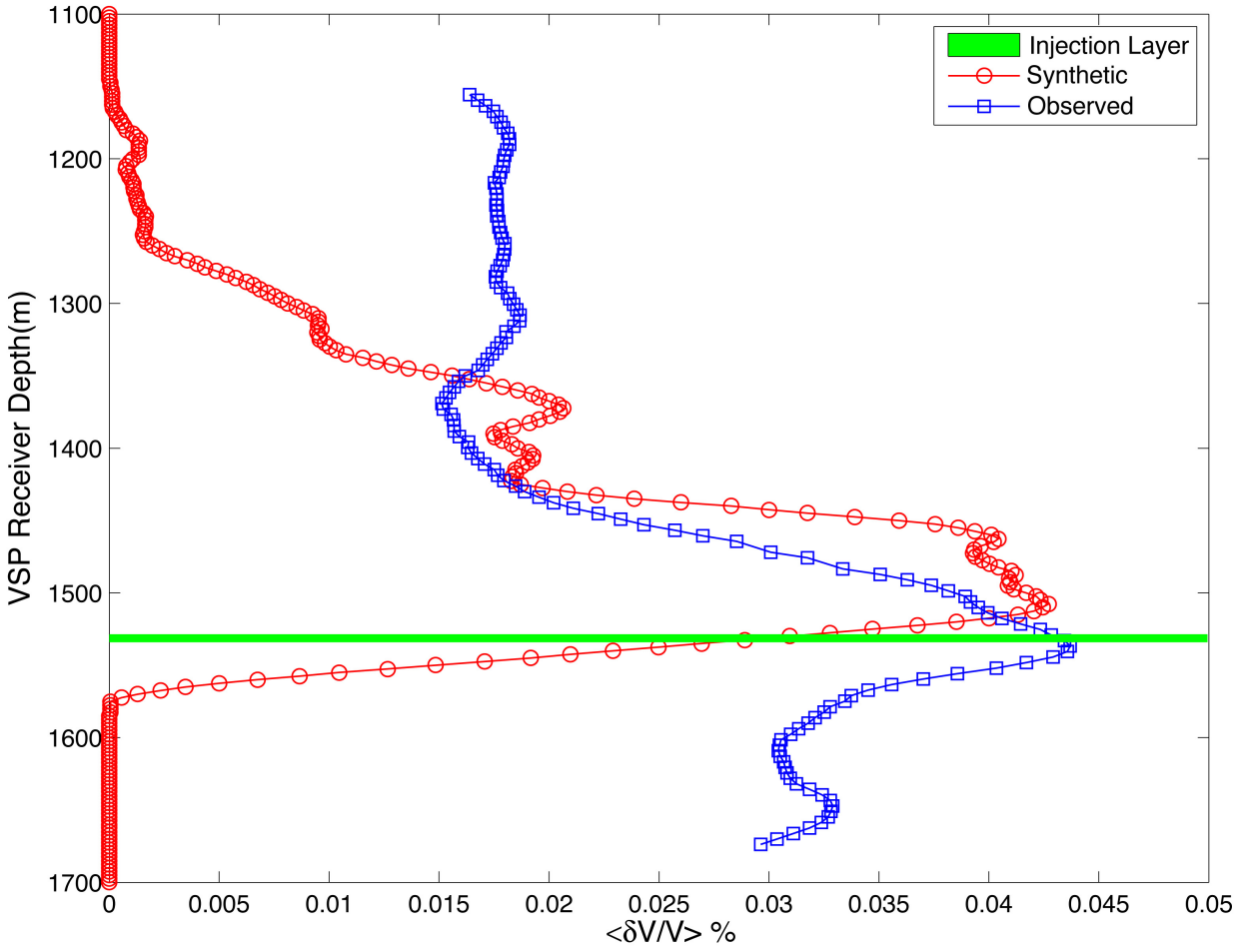
Injection Layer
Synthetic
Observed
VSP Receiver Depth(m)
1100
1200
1300
1400
1500
1600
1700
0
0.005
0.01
0.015
0.02
0.025
0.03
0.035
0.04
0.045
0.05
<δV/V> %

Figure 9.